processes

MDPI

Article

Numerical Simulation of Impinging Jet Drying Multiphase Flow in Gravure Printing Water-Based Ink Based on the Volume of Fluid Method

Hongjuan Zhu †, Jiefang Xing *,†, Wanjun Zhu and Xiaomin Guan

Co-Innovation Center of Efficient Processing and Utilization of Forest Resources, Nanjing Forestry University, Nanjing 210037, China

* Correspondence: jiefangx@njfu.edu.cn; Tel.: +86-025-85428036

† Hongjuan Zhu and Jiefang Xing contributed equally to this work and should be considered first authors.

Abstract: Gravure printing is widely used in food, pharmaceutical, and other packaging industries. As a green printing material, water-based ink has problems such as non-volatile and poor drying on non-absorbent packaging substrates, which has a great impact on its application. To solve these difficulties, this study adopts the volume of fluid (VOF) method and user-defined function (UDF) to establish a multiphase flow impinging air jets drying model of water-based ink in the gravure printing process, taking a water-based ink droplet as an example. The model was used to simulate the ink drying state in the impinging air jets region and analyze the effects of impinging air jets' temperature and velocity, as well as ink viscosity and thickness, on the ink drying efficiency. Meanwhile, the heat and mass transfer mechanism between impinging air jets and water-based ink was investigated. The results show that the higher impinging air jet temperature and velocity, the faster the drying rate of the ink; a lower viscosity and thinner thickness of ink can also enhance the drying efficiency of the ink. The multiphase impinging air jets drying model based on the computational fluid dynamics (CFD) method provides a new research idea for the analysis of drying characteristics of water-based ink on non-absorbent substrates, and the research results provide theoretical support to promote its application.

Keywords: water-based ink; impinging air jets drying; simulation; heat and mass transfer

Citation: Zhu, H.; Xing, J.; Zhu, W.; Guan, X. Numerical Simulation of Impinging Jet Drying Multiphase Flow in Gravure Printing Water-Based Ink Based on the Volume of Fluid Method. *Processes* **2023**, *11*, 847. https://doi.org/10.3390/pr11030847

Academic Editor: Yanzhen Zhang

Received: 16 January 2023
Revised: 17 February 2023
Accepted: 22 February 2023
Published: 12 March 2023

1. Introduction

Gravure printing products are characterized by vibrant color, high reproduction, and a strong three-dimensional sense. Therefore, gravure printing is suitable for continuous pattern printing and long-term investment. The major inks used for printing are solvent-based ink and water-based ink. Water-based ink is an environmentally friendly printing material with low viscosity and better flow ability. However, compared to solvent-based ink, water-based ink has problems such as non-volatile and poor drying on non-absorbent flexible packaging substrates, which limits its application. In response to the complexity and difficulties of the printing mechanism in gravure printing on non-absorbent sub-strates, the structural mechanics of gravure layout folding, ink transfer, and the fluid-solid coupling of ink transfer are investigated [1–3]. This study further explores water-based ink drying under gravure printing for systematic research.

Gravure printing usually uses hot air drying to dry the print, a method known as high-velocity impingement air jets. Drying efficiency is enhanced by using nozzles whose jet axis is perpendicular to the direction of the moving print to eject hot air onto a flat surface filled with ink. The principle of impinging air jets is to increase convection by reducing the thickness of the boundary layer. The energy provided by the drying air flow promotes the evaporation of moisture in the ink layer [4]. The high-velocity impinging air jets are used in a wide range of applications because of their ability to produce high heat

and mass transfer rates in the impinging region. For instance, they are often used in the industry to dry, cool, or heat different workpieces [5].

In multicolor printing techniques, rapid drying is particularly important because each color should be at least a touch dry before another color is successfully imprinted [6]. In the ink-drying process, mass and heat transfer are essentially simultaneous. Experimental studies on heat transfer by impinging air jets have been carried out by several scholars. They found that there is an interaction between the jets and optimized the design of the array of air impingement nozzles, which provides a foundation for the design of heat transfer devices [7,8]. To solve problems such as poor drying efficiency, some scholars developed mathematical models to analyze the heat and mass transfer in the hot air drying process of ink to predict the ink drying rate [9,10]. In these studies, the analysis of the drying process mainly focuses on the theoretical study of heat and mass transfer for ink drying and the establishment of mathematical models without fully considering the influence of the structure of the impinging air jets' drying apparatus on the drying effect.

The design of multi-nozzle drying equipment is quite complex since many factors have to be considered, such as nozzle size, shape, spacing, the distance between the nozzle and the surface, airflow velocity, and temperature. To satisfy the needs of academic and industrial applications, the flow field under impinging air jets was given by Can [11]. Hardisty and Can found that the heat transfer coefficient is maximum when eight slot widths are spaced from the nozzle surface [12]. Can et al. determined the effect of nozzle width on the heat transfer coefficient in the impingement area [13]. The effect of nozzle shape and slit width on heat transfer was studied by Etemoglu et al. It was found that better heat transfer and lower production costs can be obtained using hole arrays [14,15]. Caliskan et al. found that elliptical jets have better heat transfer performance. In addition, they performed simulations and determined the velocity distribution of the impinging air jets [16]. However, the study did not investigate the effect of airflow temperature on the heat transfer of the impinging jet and neglected the evaporation of the substance dried.

Drying technologies generally involve the evaporation of water from porous solids. The ink-drying research platform was originally constructed by Hardisty to study the drying characteristics of ink films [17]. He showed that drying takes place at a constant rate during the early stage of ink drying. During this period, approximately 80% of the solvent is removed, and the drying rate is mainly controlled by the impinging air jet conditions [6,18,19]. Moreover, some scholars determined ink-drying curves by monitoring the content of volatile solvents [20–22]. To provide data for ink dryer designers, Turkan et al. investigated the effects of air jet velocity and temperature variations on the experimental constant drying rate and falling drying time. They also surveyed published theoretical and experimental information about ink drying and briefly summarized the progress of research on impinging air jets [4,23].

When conducting practical drying experiments on water-based inks, there are difficulties in controlling the operating conditions, quantifying the experimental data due to the thin ink layer of the products, and high experimental costs. Thus, it is not convenient to study water-based ink drying from the experimental perspective, whereas this problem can be solved through the simulation method. Previous studies on the simulation of impinging air jets in gravure printing mainly focused on analyzing the distribution of impinging air jets in the drying chamber to investigate the ink-drying effect, neglecting the heat and mass transfer between the impinging air jets and the ink [24–26].

Based on the above analysis, this paper adopts ANSYS Fluent software to establish an impinging air jets drying model of water-based ink by using the volume of fluid (VOF) method and applying a user-defined function (UDF) to computational fluid dynamics (CFD) in combination with the heat and mass transfer theory of water-based ink. The viability of the simulation method was verified by comparing it with related studies. In this study, the multiphase flow drying model was developed to analyze the heat and mass transport between the impinging jets and the water-based ink and the fluid distribution on the surface of the water-based ink. Meanwhile, the effects of air temperature, air velocity, ink

viscosity, and ink thickness on the drying efficiency of water-based inks were investigated using the model. The entire research process was simulated with water-based ink droplets. The fluid dynamics simulation method proposed in this work can provide a new research idea for water-based ink drying, which facilitates the design and analysis of the drying process of water-based ink to improve the drying efficiency and promote the application of water-based ink. The design guidelines for the study are shown in Figure 1.

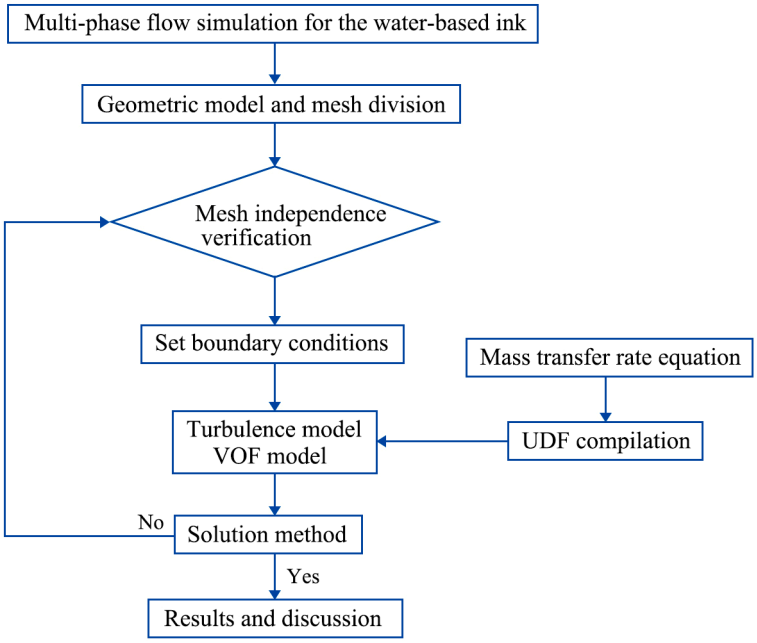

Figure 1. Framework for the study.

2. Materials and Methods

2.1. Basic Assumptions

Water-based ink is a mixture of complex substances. In fluid dynamics simulation, the following assumptions are made to simplify the analysis.

(1) The research object is a water-based ink droplet in the partial area of the print surface below a single nozzle in the gravure drying chamber, ignoring the influence of airflow from the surrounding nozzles on the water-based ink drying in the adjacent area.

(2) The movement of water-based ink and non-absorbent substrates is not considered. As shown in [27], the surface movement can be ignored when the surface linear velocity is less than 20% of the impinging jet velocity.

(3) It is assumed that water-based ink is a well-distributed substance and that the final thickness of the ink layer is equal after drying water-based ink. Consequently, the influence of solid phases in the ink composition, such as pigments, dyes, and binders, on the aqueous ink drying is neglected.

(4) The effect of the substrate thickness and the heat transfer characteristics of the surface on the drying of water-based ink is ignored. Meanwhile, water-based ink is regarded as a single-component substance.

(5) Since water evaporation plays a predominant role in the drying effect of water-based ink, this paper only considers the evaporation of water in water-based ink, ignoring the influence of other solvents.

2.2. Fluid Mechanics Theoretical Foundation

2.2.1. Fluid Mechanics Control Equations

The impinging air jets in the gravure drying chamber is a fully developed turbulent flow, which is represented by the Navier–Stokes equation as follows:

$$\rho \frac{Dv}{Dt} = \rho f - \nabla p + \mu \nabla^2 v \tag{1}$$

where ρ is the fluid density, t is the time, v is the velocity vector, p is the pressure, f is the external force per unit volume of fluid, and μ is the dynamic viscosity coefficient constant.

In the drying process, heat is transmitted to the surface of the water-based ink through the hot air while prompting the solvent to evaporate from the water-based ink. The entire process obeys the law of energy conservation, and the energy conservation equation is as follows:

$$\frac{\partial(\rho T)}{\partial t} + \frac{\partial(\rho u T)}{\partial x} + \frac{\partial(\rho v T)}{\partial y} + \frac{\partial(\rho w T)}{\partial z} = \frac{\partial}{\partial x}\left(\frac{k_1}{c_p}\frac{\partial T}{\partial x}\right) + \frac{\partial}{\partial y}\left(\frac{k_1}{c_p}\frac{\partial T}{\partial y}\right) + \frac{\partial}{\partial z}\left(\frac{k_1}{c_p}\frac{\partial T}{\partial z}\right) + S_T \tag{2}$$

where c_p is the specific heat capacity; T is the temperature; k_1 is the heat transfer coefficient of the fluid; S_T is the viscous dissipation term and u, v, and w are the components of the velocity vector in the x, y, and z directions, respectively.

The whole drying process also follows the law of mass conservation, and the mass conservation equation is described as follows:

$$\frac{\partial \rho}{\partial t} + \nabla \cdot (\rho v) = 0 \tag{3}$$

In this research, the standard $k - \varepsilon$ model is used to solve the flow and heat transfer problems. The turbulent kinetic energy k and dissipation rate ε equations of the standard $k - \varepsilon$ equation can be written as:

$$\frac{\partial(\rho k)}{\partial t} + \frac{\partial(\rho k u_i)}{\partial x_i} = \frac{\partial}{\partial x_j}\left[\left(\mu + \frac{\mu_t}{\sigma_k}\right)\frac{\partial k}{\partial x_j}\right] + G_k + G_b - \rho\varepsilon - Y_M \tag{4}$$

$$\frac{\partial(\rho \varepsilon)}{\partial t} + \frac{\partial(\rho \varepsilon u_i)}{\partial x_i} = \frac{\partial}{\partial x_j}\left[\left(\mu + \frac{\mu_t}{\sigma_\varepsilon}\right)\frac{\partial \varepsilon}{\partial x_j}\right] + C_{1\varepsilon}\frac{\varepsilon}{k}(G_k + C_{3\varepsilon}G_b) - C_{2\varepsilon}\rho\frac{\varepsilon^2}{k} \tag{5}$$

where G_k is the turbulent energy due to the mean velocity gradient; G_b is the turbulent energy due to the buoyancy effect; Y_M is the effect of compressible turbulent pulsation expansion on the total dissipation rate; $C_{1\varepsilon}$, $C_{2\varepsilon}$, and $C_{3\varepsilon}$ are empirical constants; and σ_k and σ_ε are the Prandtl numbers corresponding to both the turbulent energy k and the dissipation rate ε, respectively.

The turbulent viscosity is expressed as a function of the turbulent energy k and the dissipation rate ε:

$$\mu_t = \rho C_\mu \frac{k^2}{\varepsilon} \tag{6}$$

where C_μ is an empirical constant.

2.2.2. Volume of Fluid Method

The VOF model tracks the amount of fluid in each computational cell grid by the volume of fluid function to obtain the interface shape between two or more mutually immiscible fluids, which captures a clear intersection interface. Due to the requirement for a clear gas–liquid interface to define the evaporative state of water-based ink, the VOF model is adopted to solve the multiphase flow in this paper. The phases included in the drying process are dry air (gas phase), water vapor (gas phase), and water-based ink droplet (liquid phase). In the VOF model, all fluid phases share the same set of momentum

equations, and the volume fraction of each fluid phase is recorded in each computational cell across the computational domain. Moreover, the sum of the volume fractions for these phases in each computational cell is 1. The interface between the gas–liquid phases is tracked by solving the volume fraction equation, which for the qth phase is represented by

$$\frac{\partial \alpha_q}{\partial t} + v \cdot \nabla \alpha_q = 0 \tag{7}$$

The volume fraction between the three phases is bounded by the following equation:

$$\sum_{q=1}^{3} \alpha_q = 1 \tag{8}$$

where α_q is the volume fraction of the qth phase in the calculation cell.

2.3. Heat and Mass Transfer of Water-Based Ink

2.3.1. Mass Transfer of Water-Based Ink

The mass transfer of water-based ink is firmly related to the difference in concentration of solvent vapor on its surface. During the ink drying process, the heat transfer of water-based inks varies, which in turn generates a mass transfer between the water-based ink and the impinging air jets. On the surface of the water-based ink, the vapor concentration of the solvent is the highest, while the lowest concentration is in the drying air. The solvent vapor is transported to the drying air due to its concentration difference and then flows out with the impinging air jets. The constant velocity flow of solvent vapor on the surface of the water-based ink can be characterized by the mass transfer rate equation:

$$\dot{m} = h' A_s \left(P_{surf} - P_{air} \right) \tag{9}$$

where h' is the mass transfer coefficient, and the empirical coefficient of evaporation for water solvent in this study is 0.04 [28]; A_s is the surface area; P_{surf} is the saturated vapor pressure of pure solvent; and P_{air} is the partial pressure of the solvent in drying air.

The relationship between P_{surf} and the absolute temperature T can be represented as [19]

$$\log P_{surf} = A - B/T \tag{10}$$

where A and B are constants.

In this research, only pure water solvent is considered, and the effect of other trace solvents is neglected. If the printing material used is a nano-ink, which contains nanoscale particles, the aqueous solvent will behave like a liquid in nanometer-diameter capillaries. The saturated vapor pressure over the curved surface of the water meniscus in the capillary is always lower than the saturated vapor pressure over a flat water surface. In this case, the solvent saturation vapor pressure can be appropriately corrected by the Kelvin equation [29]:

$$\ln\left(P/P_{surf} \right) = (M/RT\rho_1)(2s/r) \tag{11}$$

where P is the vapor pressure over the curved surface, M is the molar mass, R is the universal gas constant, ρ_1 is the solvent density, s is the surface tension coefficient, and r is the radius of curvature of the liquid surface in a capillary.

For the common ink without nanoscale particles, the relationship between P_{surf} and absolute temperature T at this point can be expressed as [30]:

$$\lg P_{surf} = 7.07406 - \frac{1657.46}{T + 227.02} \tag{12}$$

The applicable range of T is 10~168 °C.

2.3.2. Heat Transfer of Water-Based Inks

During the drying process, heat is transferred to the surface of the ink, while solvent vapors are transferred from the surface of the water-based ink. The heat supplied can be used both for evaporating the solvent and for dynamic energy balance, the equation of which is

$$h' A_s \left(P_{surf} - P_{air} \right) h_{fg} + \frac{m c_p \Delta T}{\Delta t} \tag{13}$$

where m is the mass of the ink/solvent, ΔT is the temperature change of the ink/solvent, and h_{fg} is the evaporation enthalpy of the solvent. At equilibrium, the energy gained in the form of heat is exactly enough to vaporize the solvent.

2.4. Boundary and Initial Conditions

In this paper, the effect of vertical downward gravity is considered, taking a water-based ink droplet with a radius of 20 μm for the simulation. Due to the similarity of the structure in the impinging jet nozzles in the gravure drying chamber, the selected calculation domain is the partial unit below one of the nozzles near the surface of the substrate to reduce the calculation time. At initial conditions, the computational domain consists of the air phase and the liquid phase with the water-based ink, with drying air surrounding the droplet. The calculation domain is shown in Figure 2, where the boundaries are marked. At boundaries 2 and 4, the initial air pressure is zero (gauge pressure). Additionally, boundary 1 is the inlet boundary, and boundary 3 is the no-slip, no-permeation, thermal insulation wall boundary. Moreover, the width of boundaries 1 and 3 is 2000 μm, and the height of boundaries 2 and 4 is 1000 μm. A rectangular grid with a uniform size of 5 μm is adopted throughout the computational domain for the model.

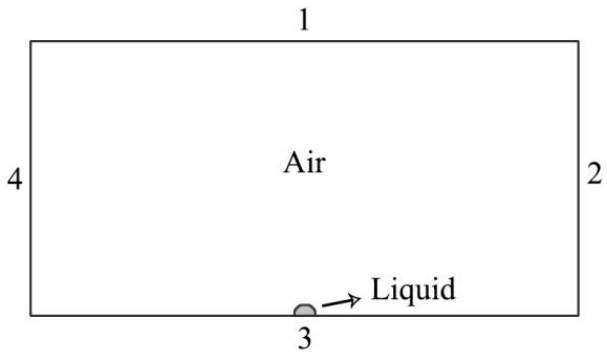

Figure 2. Geometry of the computational domain.

The initial conditions and material parameters of the model for the water-based ink drying are shown in Tables 1 and 2, respectively.

Table 1. Initial conditions for the drying of water-based ink droplets.

Variable	Instruction	Value
D_{liq}	Droplet diameter	20 μm
T_{air}	Impinging jet temperature	65 °C
T_{liq}	Droplet temperature	20 °C
V_{air}	Impinging jet velocity	25 m/s
P_{air}	Impinging jet pressure (gauge)	0 Pa
P_{liq}	Droplet pressure (gauge)	0.2 Pa

Table 2. Material parameters.

Variable	Description	Value
$c_{p,\text{air}}$	Specific heat of air	1006.43 J/kg-k
$c_{p,\text{liq}}$	Specific heat of liquid	4182 J/kg-k
$c_{p,\text{vap}}$	Specific heat of vapor	1840 J/kg-k
ρ_{air}	Density of air	1.225 kg/m^3
ρ_{liq}	Density of liquid	998.2 kg/m^3
ρ_{vap}	Density of vapor	0.5542 kg/m^3
k_{air}	Thermal conductivity of air	0.0242 w/m-k
k_{liq}	Thermal conductivity of liquid	0.6 w/m-k
k_{vap}	Thermal conductivity of vapor	0.0261 w/m-k
vis_{air}	Viscosity of air	1.7894×10^{-5} Pa·s
vis_{liq}	Viscosity of liquid	0.0356 Pa·s
vis_{vap}	Viscosity of vapor	1.34×10^{-5} Pa·s
S	Surface tension of liquid	0.04 N/m

2.5. Solution Method

Numerical simulation was performed using ANSYS Fluent software, based on the SIMPLEC (Semi-Implicit Method for Pressure-Linked Equations—Consistent) algorithm using a pressure–velocity coupled solver for the computational solution. Meanwhile, the simulation was conducted in transient state mode to better obtain the drying time required for water-based ink under different conditions. Since impinging airflow in the gravure tumble dryer is turbulent, the standard $k-\varepsilon$ turbulence model was adopted in this study, and the VOF model was applied to track the volume fraction changes in drying air, liquid phase, and water vapor. In addition, Equations (9) and (12) were compiled as UDF to explore the heat and mass transfer for water-based ink drying. Based on the Eulerian method, a least squares cell (LSC) was employed for spatial discretization, while the time scheme was in first-order implicit form. Furthermore, the momentum and energy were discretized using the second-order windward method. The volume fraction, turbulent kinetic energy, and turbulent dissipation rate were used in the first-order windward format.

3. Model Verification

3.1. Grid-Independent Validation

In simulation processes, the number of grids is crucial because it will affect the accuracy of the calculation results. If the number of grids is too few, the research tolerance will be too large, and the accuracy of the simulation will not be achieved. On the contrary, too many meshes will cause the computation time to be excessive, increasing the burden on the computer and even making it impossible to compute properly. To enhance the mesh quality and avoid the influence of the mesh quantity on the calculation results during the simulation as much as possible, it is necessary to verify the irrelevance of the mesh quantity.

As the drying effect of water-based ink is closely related to the temperature of the drying air, this study selected different numbers of grids to examine the surface temperature of water-based ink to ensure that the relative tolerance of the simulation is minor. The results are shown in Figure 3. It can be noticed that the simulation results do not vary widely after the number of meshes exceeds 70,000. In this paper, a mesh of 80,000 was taken to ensure the calculation accuracy and to decrease the calculation time as much as possible.

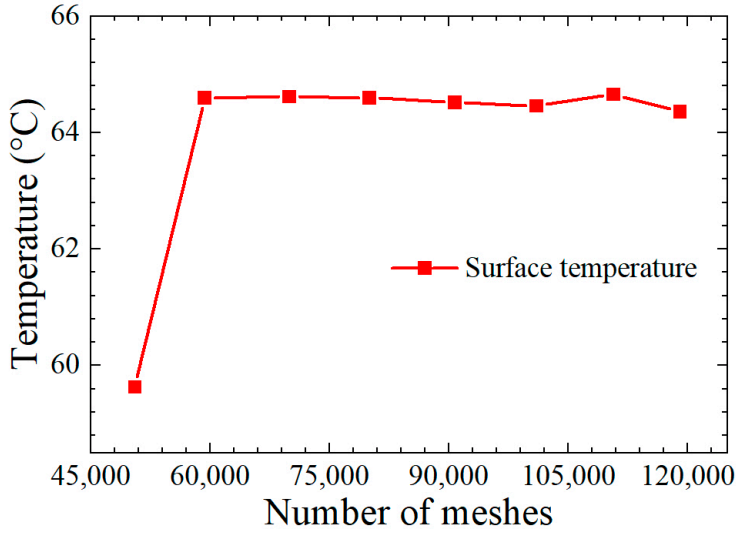

Figure 3. Verification of grid independence.

3.2. Model Verification

When T_{air} = 65 °C, V_{air} = 25 m/s, and the initial temperature of water-based ink t = 20 °C, the water-based ink drying curve obtained by the model is shown in Figure 4. It can be found in the drying curve obtained is divided into three stages. In the first stage of water-based ink, evaporation is not obvious, and the drying rate is low but presents a gradually accelerated state. After a shorter period in the first stage, the water-based ink drying moves into the constant velocity drying stage, when the drying rate of water-based ink hardly varies and becomes faster. In the last stage, the drying rate of water-based ink slowly diminishes, which indicates that the water-based ink drying has entered a decreasing drying stage. The results received from the simulation are consistent with the basic ink-drying curve experimentally determined by the research scholars [23], suggesting that the research method is feasible.

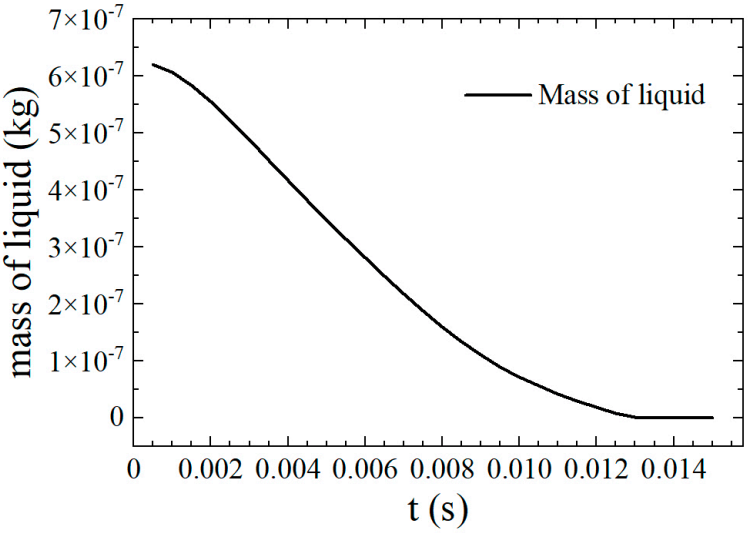

Figure 4. Drying curve of water-based ink.

4. Results and Discussion

The ingredients of water-based ink are quite complex. The evaporation effect of water-based ink is influenced by solvents such as water and ethanol, in which water evaporation plays a primary role in water-based ink drying. Due to the disadvantages that moisture

is relatively substantial in water-based ink and has less evaporation compared to organic solvents, this study assumes that the water-based ink is a uniformly dispersed single substance, with the viscosity of the water-based ink as a physical parameter to measure its state.

During the simulation, the impinging jets flow through the inlet boundary at a certain velocity and temperature, then contact the surface of the water-based ink droplet, which makes the water-based ink experience phase change by heating, thus forming the heat and mass transfer between the jets and the water-based ink. In the case of T_{air} = 65 °C, V_{air} = 25 m/s, and the initial temperature of water-based ink droplets t = 20 °C, when the drying time is t = 0 s, 0.004 s, and 0.008 s, the volume fraction of the water-based ink droplet is shown in Figure 5.

It can be observed that with increasing time, the volume fraction of the water-based ink droplet gradually decreases, which indicates that heat and mass transfer occurs between the impinging jets and the water-based ink. Fluid dynamics processes result in heat transfer across the temperature difference and mass transfer over the concentration difference [31]. This is because the airflow comes into contact with the surface of the water-based ink after entering the drying chamber, which results in heat transfer to the water-based ink, causing a mass transfer between them. During this period, the moisture in the water-based ink phase is converted from the liquid phase to the gas phase, and then the drying of water-based ink volatilization is completed. The evaporated vapor flows out with the impinging jets.

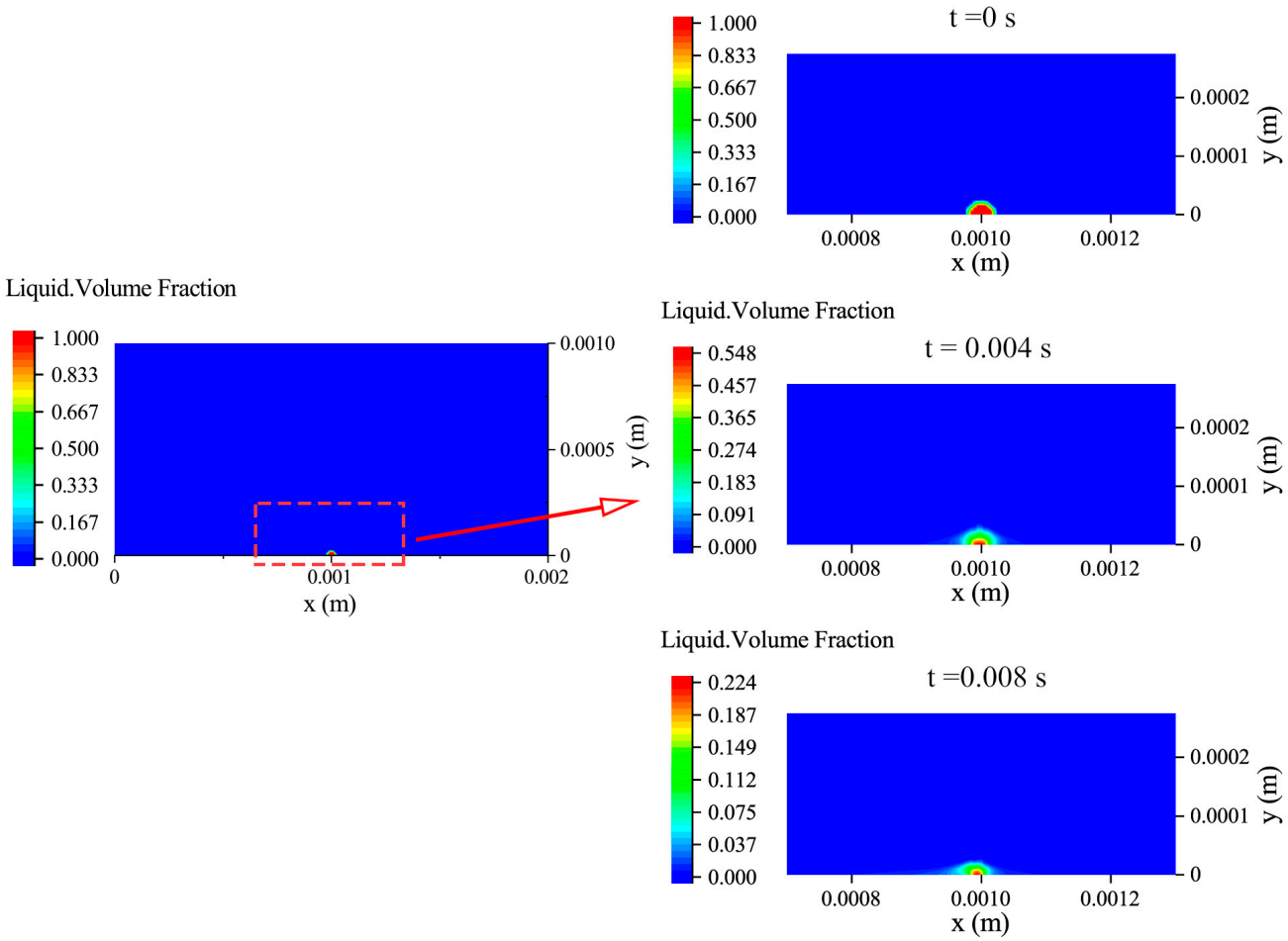

Figure 5. Variation in volume fraction of the water-based ink droplet at different times.

4.1. The Effect of Hot Air on the Drying Effect of Water-Based Ink

4.1.1. The Influence of Hot Air Temperature on the Drying of Water-Based Ink

To better understand the effect of impinging jet temperature on the drying efficiency of water-based ink, the drying process was simulated by using the established model when the air temperature T_{air} was 55, 60, 65, 70, 75, and 80 °C. The variation in drying time for water-based ink with impinging jet temperature is shown in Figure 6.

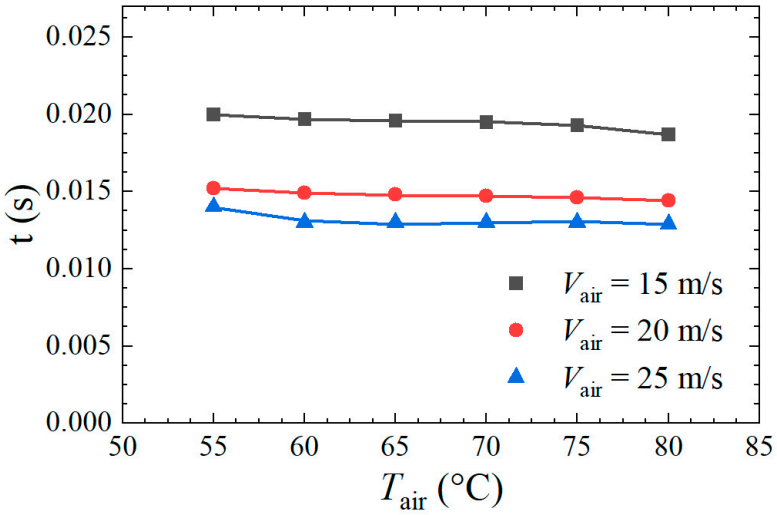

Figure 6. Variation in drying time for water-based inks with airflow temperature.

The results indicate that the drying time of water-based ink decreased with the increase in airflow temperature, which is similar to the findings of Avci et al. [10] When T_{air} = 70 °C, it can reduce the drying time of water-based ink as well as decrease heat consumption. The reason for this variation is attributed essentially to the fact that there is a wide difference between the airflow temperature and the initial temperature of the water-based ink. Being influenced by the temperature difference between them, the heat transfer from the hot air to the water-based ink in the initial period of drying raises the temperature of the water-based ink rapidly. After the temperature of the water-based ink increases, its moisture is continuously vaporized.

Due to the turbulent flow of impinging air jets in the gravure drying chamber, a fluid boundary layer is formed on the print surface. This layer of slow-moving fluid has an obstructive impact on the heat and mass transfer of the water-based ink [5]. Based on this, T_{air} was selected at 65 °C and V_{air} = 25 m/s to observe the temperature distribution around the water-based ink droplet at different times t = 0.004 s and 0.008 s, as shown in Figure 7. It can be noted that there is a temperature boundary layer on the surface of the water-based ink within the flow field, which hinders the heat exchange between the impinging jets and the water-based ink. In the drying process of water-based ink, the thickness of the boundary layer is required to be reduced as far as possible. In the selection of drying temperature, the infinite increase in drying temperature can not only be considered, but a comprehensive consideration of energy consumption and the heat resistance of the substrate must be performed as well.

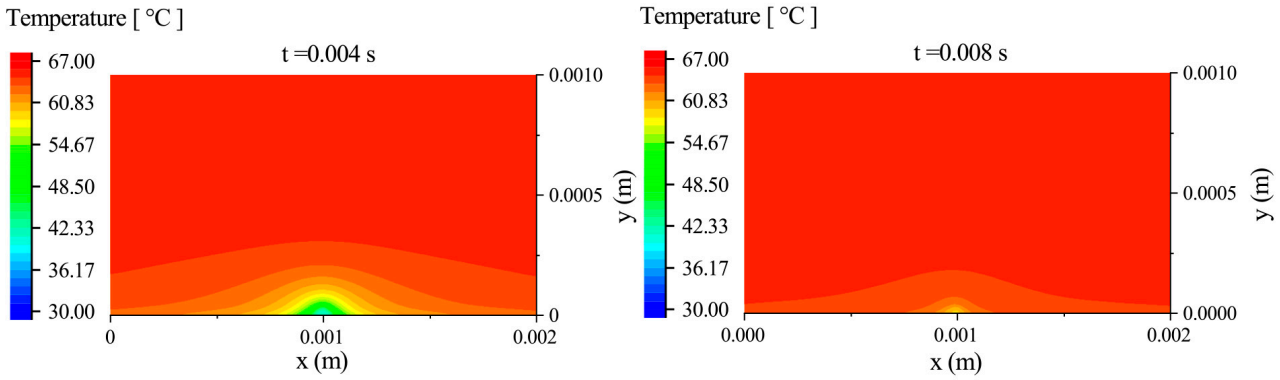

Figure 7. Distribution of temperature around the water-based ink droplet at different times.

As shown in Figure 8, the closer the impinging air jets are to the droplet of water-based ink, the lower the temperature of the airflow; the closer the inlet and outlet, the higher the temperature of the airflow. This is because heat transfer takes place between the forced convection and the water-based ink. The impinging hot airflow is ejected onto the print surface, raising the droplet temperature while the airflow temperature near the droplet surface decreases. The hot jet continuously transfers heat to the water-based ink, and the ink temperature gradually increases during the drying process. The numerical simulation results reflect a good heat exchange between the impinging air jets and the water-based ink.

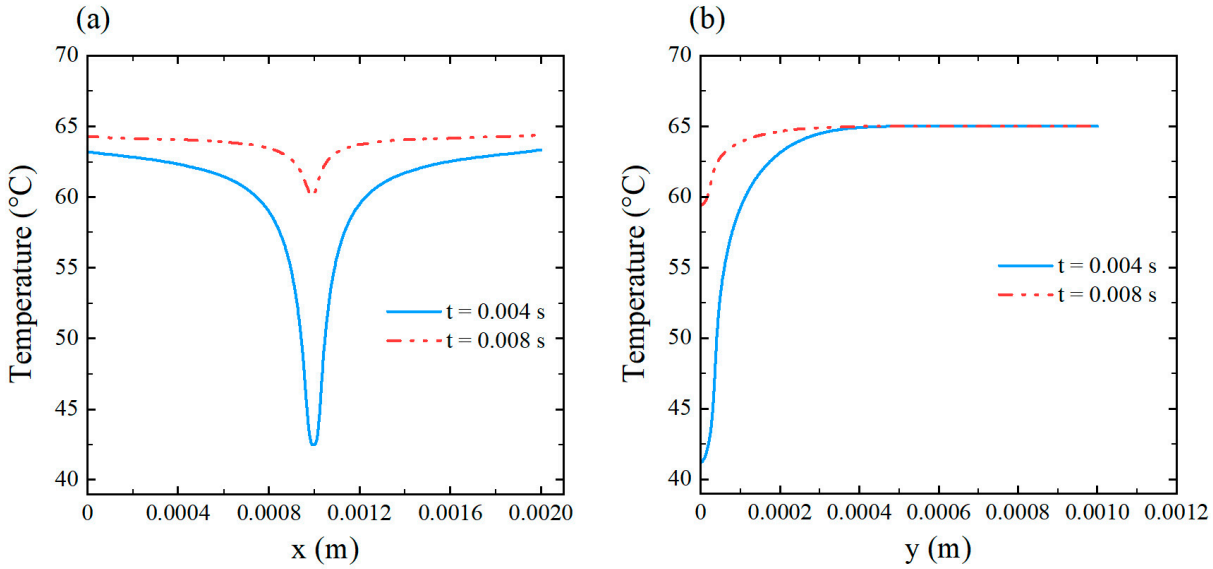

Figure 8. Distribution of temperature around the water-based ink droplet at y = 2 × 10^{-5} m (**a**) and x = 0.001 m (**b**).

4.1.2. The Influence of Hot Air Velocity on the Drying of Water-Based Ink

In the actual gravure printing process, the velocity of impinging air jets is commonly in the range of 15~35 m/s. When the water-based ink viscosity was 0.04 Pa·s, 0.06 Pa·s, and 0.08 Pa·s, respectively, the inlet air velocity V_{air} = 10 m/s, 15 m/s, 20 m/s, 25 m/s, 30 m/s, and 35 m/s were selected for this study, in which the ink drying time was calculated to investigate the effect of different inlet air velocities on the drying effect of water-based ink. The drying curve with the variation of velocity for the drying time of water-based ink obtained from the research is illustrated in Figure 9.

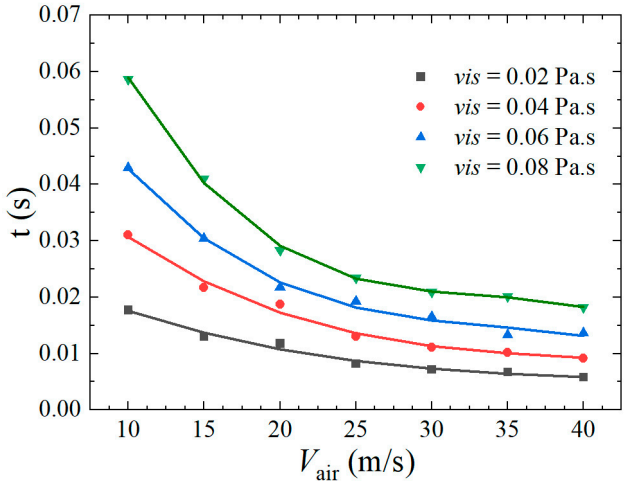

Figure 9. Variation in drying time with velocity for water-based ink (T_{air} = 70 °C).

The results show that the drying time decreases faster with the increase in impinging air jet velocity when the velocity is 10~25 m/s. However, the variation gradually tends to be smooth when the velocity is greater than 25 m/s. The above characteristics are consistent with the findings of Turkan et al. [4]. The reason for this is that the increase in the impinging airflow velocity contributes to the water solvent evaporating more quickly from the droplet surface and being rapidly carried away by the drying air, thus increasing the contact between the droplet surface and the impact airflow as well as promoting the heat and mass transfer between them. Therefore, increasing the airflow velocity can improve the drying efficiency of water-based ink. However, when the airflow velocity increases to a certain extent, the surface heat exchange between the airflow and the aqueous ink almost reaches the maximum. The effect of impinging airflow velocity on the water-based ink drying efficiency is no longer obvious at this stage.

The results indicate that the notion of the greater the drying velocity, the better the water-based ink drying is untrue. However, the process cost should be considered according to the experimental results and empirical parameters, and one should choose the appropriate airflow speed. If the optional inlet air velocity is too high, it will increase unnecessary energy consumption, and printing costs, resulting in a waste of resources. Meanwhile, if the inlet air velocity is too little, it will slow down the printing and drying efficiency of production.

On this foundation, the distribution of velocity around the droplet was observed at different times t = 0.004 s and 0.008 s for T_{air} selected as 65 °C, as shown in Figures 10 and 11. The boundary layer exists on the surface of the water-based ink when the impinging air jet dries the water-based ink. There are vortexes on the surface of the water-based ink near the exit as a result of the turbulence of the airflow.

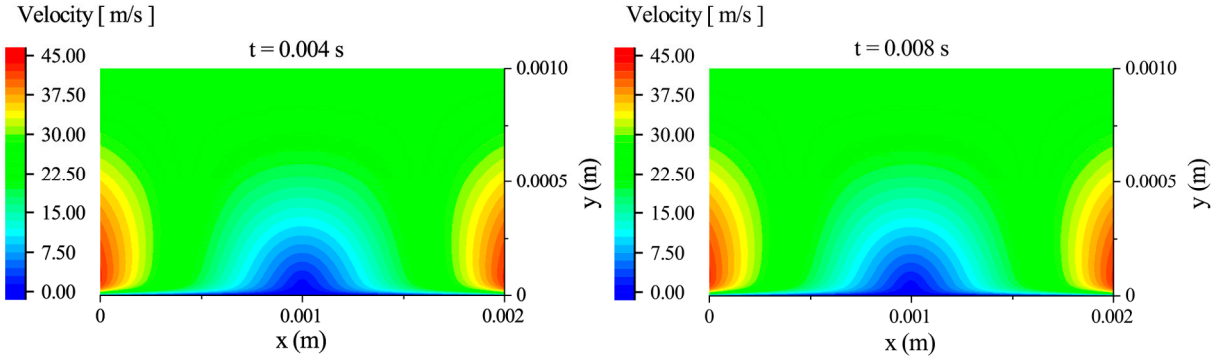

Figure 10. The velocity contour of the water-based ink drying.

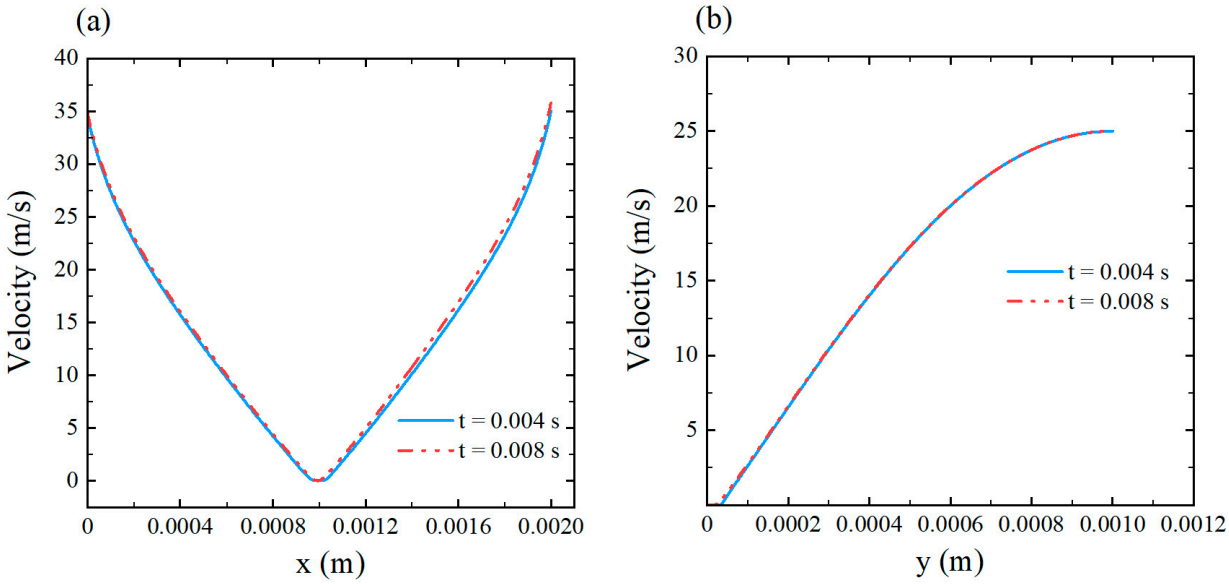

Figure 11. Distribution of velocity near the water-based ink droplet at y = 2 × 10^{-5} m (**a**) and x = 0.001 m (**b**).

It is shown in Figure 11 that due to the boundary layer, the closer the impinging jet is to the droplet, the lower the velocity of the jet; the greater the closeness between the inlet and outlet, the higher the velocity of the jet. It can be found that the drying time decreases with the increase in impinging velocity, indicating that the increase in airflow velocity is beneficial to reduce the thickness of the boundary layer. The existence of the boundary layer is not conducive to water-based ink drying. Therefore, the thickness of the boundary layer should be minimized during the ink-drying process to improve the drying efficiency by increasing the contact between the impinging jet and the water-based ink.

4.2. The Effect of Water-Based Ink Properties on Its Drying Efficiency

4.2.1. The Influence of Water-Based Ink Viscosity

The water-based ink viscosity also affects the drying efficiency of water-based ink. In this research, the drying effect of water-based ink viscosity at different air velocities was investigated. The water-based ink viscosity was selected for 0.02~0.08 Pa·s with the velocity of V_{air} = 15 m/s, 20 m/s, and 25 m/s, respectively. The drying time with the water-based ink viscosity is depicted in Figure 12.

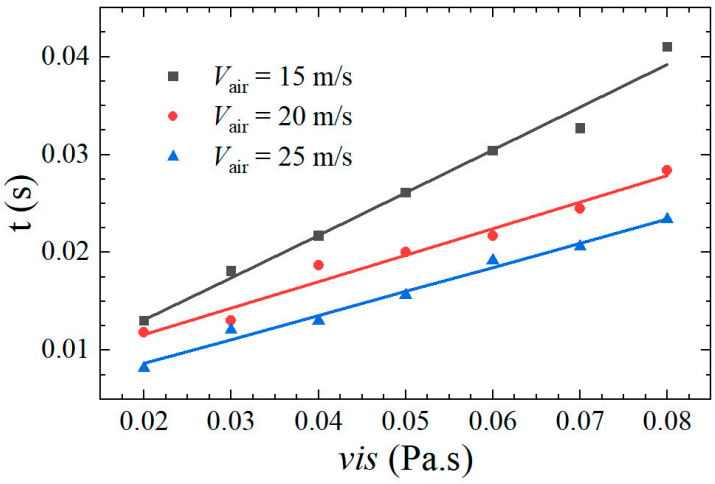

Figure 12. Variation in drying time with water-based ink viscosity.

It can be found that as the water-based ink viscosity increases, the drying time of the water-based ink also prolongs. This is due to the water-based ink viscosity having a certain influence on the intermolecular force of water-based ink. The lower the water-based ink viscosity, the weaker the intermolecular forces. Therefore, it is easier to separate the water molecules from the water-based ink, which makes the water-based ink more effective in drying. The print coloring performance is also affected by the water-based ink viscosity. When the water-based ink viscosity is too little, the print brightness will be degraded. On the contrary, if the water-based ink viscosity is too big, it will decrease the transfer efficiency of water-based ink in printing. As are result, the water-based ink viscosity is supposed to be reasonably controlled.

4.2.2. The Influence of Ink Thickness on the Drying of Water-Based Ink

In the actual production process, staff should choose the appropriate gravure printing hole depth according to the ink transfer rate to achieve control of the ink thickness. This research investigated the changed regulation of the drying time for water-based ink at different ink thicknesses. A simulation was conducted to measure the drying time at different ink thicknesses of 10 μm, 15 μm, 20 μm, 25 μm, and 30 μm with the air velocities of V_{air} = 15 m/s, 20 m/s, and 25 m/s. The variation in the drying time with the water-based ink thickness is shown in Figure 13.

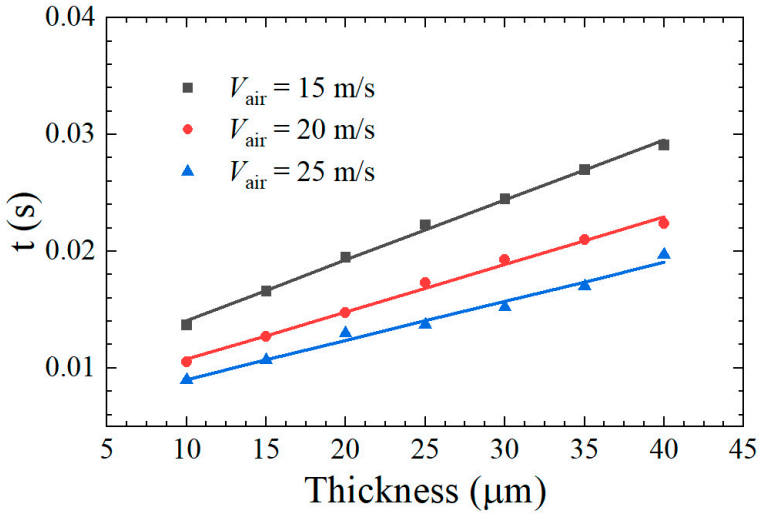

Figure 13. Variation in drying time with water-based ink thickness.

The results suggest that as the thickness of the ink layer increases, the drying time of the water-based ink increases almost proportionally. This is because the thickening of the ink layer hinders the heat transfer from the impact airflow to the inside of the ink layer. Then, more heat is necessary to evaporate the water-based ink, which reduces the drying efficiency. Therefore, the drying speed of water-based ink decelerates for thicker ink layers.

It can be concluded that the water-based ink thickness is an important factor affecting the drying effect. Moreover, the thinner the thickness of the water-based ink, the more conducive it is to water-based ink evaporation. In practice, the thickness of the printed ink layer cannot be infinitely reduced because if the thickness of the ink layer is too thin, it will reduce the printing color on the printing product quality. Therefore, it is necessary to decrease the ink thickness under the condition of meeting the printing quality requirements.

4.3. Overall Discussion

The model established has some limitations of applicability due to the assumptions made in the study. First of all, the model developed does not apply to water-based inks containing nanomaterials because the saturation vapor pressure of the solvent is not corrected in the UDF, but only to common water-based inks containing solid particles such

as dye particles and pigment particles of micron scale. In the second place, the water-based ink thickness is supposed to be no less than 10 μm when it is transferred from the printing plate cavity to the print surface. The reason for this is that if the water-based ink thickness is too thin, a more detailed grid will be required, which will aggravate the computational burden as a result of computational simulation not being carried out smoothly. In the end, this research regards the water-based ink as stationary during drying; hence, the application of this model ought to ensure that the ratio of jet velocity to printing speed is greater than or equal to 5 m/s. Therefore, the range of jet velocity is 10~45 m/s.

5. Conclusions

Combining the VOF method and the UDF formed by applying the mass transfer rate equation of water-based ink through the CFD method, a new multiphase flow model for drying water-based inks was developed in this study, which was used to examine the influence of impinging airflow and the basic properties of water-based ink on the drying effect of water-based ink.

(1) The results show that both the airflow conditions and water-based ink properties have important effects on the drying of water-based ink. Increasing impinging jet temperature, impinging jet velocity, and decreasing the viscosity and thickness of water-based ink can improve the drying effect of water-based ink.

(2) The preliminary prediction of the drying effect of water-based inks can be achieved by using the established multiphase flow model for water-based ink drying to economize the actual drying experiment time of water-based ink, reduce production costs, and improve printing efficiency.

(3) The simulation method of compiling the water-based ink mass transfer rate equation into UDF through the CFD approach opens up a new way for the research of water-based ink drying, which has great significance for solving the problem of drying difficulties of water-based ink on non-absorbent flexible packaging substrates and promoting the application of water-based ink.

Future work will investigate complex gas–liquid–solid coupling by considering the cured film formation of the water-based ink. Detailed error analysis will be performed by actual experimental verification in the printing factory.

Author Contributions: Methodology, H.Z. and J.X.; software, H.Z. and J.X.; validation, H.Z., J.X. and W.Z.; formal analysis, H.Z.; investigation, H.Z. and J.X.; resources, J.X.; data curation, H.Z.; writing—original draft preparation, H.Z.; writing—review and editing, H.Z., J.X., W.Z. and X.G.; visualization, H.Z.; supervision, J.X.; H.Z. and J.X. contributed equally to this work and should be considered first authors. All authors have read and agreed to the published version of the manuscript.

Funding: This research received no external funding.

Institutional Review Board Statement: Not applicable.

Informed Consent Statement: Not applicable.

Data Availability Statement: The data presented in this study are available on request from the corresponding author.

Conflicts of Interest: The authors declare no conflict of interest.

References

1. Wu, S.; Xing, J.; Dong, L.; Zhu, H. Multi-Objective Optimization of Microstructure of Gravure Cell Based on Response Surface Method. *Processes* **2021**, *9*, 403. [CrossRef]
2. Dong, L.; Xing, J.; Wu, S.; Guan, X.; Zhu, H. Simulation of Shear-Thickening Liquid Transfer between U-Shaped Cell and Flat Plate. *Processes* **2021**, *9*, 838. [CrossRef]
3. Guan, X.; Xing, J.; Zhu, H.; Zhu, W. Numerical simulation of the water-based ink transfer process in roll-to-roll gravure printing based on fluid–solid interactions. *AIP Advances* **2022**, *12*, 75015. [CrossRef]
4. Turkan, B.; Etemoglu, A.B.; Can, M. An investigation into evaporative ink drying process on forced convective heat and mass transfer under impinging air jets. *Heat Mass Transf.* **2019**, *55*, 1359–1369. [CrossRef]

5. Avci, A.; Can, M. The analysis of the drying process on unsteady forced convection in thin films of ink. *Appl. Therm. Eng.* **1999**, *19*, 641–657. [CrossRef]
6. Hardisty, H. Analysis of the constant rate period of ink drying. *J. Oil Colour Chem. Assoc.* **1977**, *60*, 479–487.
7. Gardon, R.; Akfirat, J.C. Heat transfer characteristics of impinging two-dimensional air jets. *J. Heat Transf.* **1966**, *88*, 101–107. [CrossRef]
8. Can, M. Simultaneous convective heat and mass transfer in impingement ink drying. *Int. Commun. Heat Mass Transf.* **1998**, *25*, 863–874. [CrossRef]
9. Jia, C.J.; Chen, G.X.; Li, X.Z. Research on the mathematical model and air-drying mechanism of water-based ink. *Adv. Mater. Res.* **2010**, *174*, 381–384. [CrossRef]
10. Avci, A.; Can, M.; Etemoglu, A.B. A theoretical approach to the drying process of thin film layers. *Appl. Therm. Eng.* **2001**, *21*, 465–479. [CrossRef]
11. Can, M. An Investigation into the Heat Transfer Characteristics of Single and Multiple Impinging Air Jets. Master's Thesis, University of Bath, Bath, UK, 1981.
12. Hardisty, H.; Can, M. An experimental investigation into the effect of changes in the geometry of a slot nozzle on the heat transfer characteristics of an impinging air jet. *Proc. Inst. Mech. Eng. Part C* **1983**, *197*, 7–15. [CrossRef]
13. Can, M.; Etemoglu, A.B.; Avci, A. Experimental study of convective heat transfer under arrays of impinging air jets from slots and circular holes. *Heat Mass Transf.* **2002**, *38*, 251–259. [CrossRef]
14. Etemoglu, A.B.; Can, M. Performance studies of energy consumption for single and multiple nozzle systems under impinging air jets. *Heat Mass Transf.* **2013**, *49*, 1057–1070. [CrossRef]
15. Etemoglu, A.B.; Isman, M.K.; Can, M. Investigation into the effect of nozzle shape on the nozzle discharge coefficient and heat and mass transfer characteristics of impinging air jets. *Heat Mass Transf.* **2010**, *46*, 1395–1410. [CrossRef]
16. Caliskan, S.; Baskaya, S.; Calisir, T. Experimental and numerical investigation of geometry effects on multiple impinging air jets. *Int. J. Heat Mass Transf.* **2014**, *75*, 685–703. [CrossRef]
17. Hardisty, H. An Investigation into the Drying of Thin Films of Ink Using Infra-Red Dryness Measurement. Ph.D. Thesis, University of Bath, Bath, UK, 1980.
18. Hardisty, H. *The Analysis of the Drying Process in Thin Films of Ink, Proc. First Int. Symposium on Drying*; Science Press Princeton: Princeton, USA, 1978; pp. 208–215.
19. Hardisty, H. Evaporative Drying Using Impinging Air Jets. In Proceedings of the International Conference on Market Trends and Technical Developments in Gravure, Gravure, Pira, 1–16 September 1980.
20. Black, J.; Hardisty, H. Heat and mass transfer in ink drying and infra-red dryness measurement. In *Thermodynamics and Fluid Mechanics: Convention Proceedings*; Mechanical Engineering Publishing: Durham, NC, USA, 1977; pp. 99–108.
21. Weyermann, C.; Kirsch, D.; Vera, C.C.; Spengler, B. A GC/MS study of the drying of ballpoint pen ink on paper. *Forensic Sci. Int.* **2007**, *168*, 119–127. [CrossRef] [PubMed]
22. Cantu, A.A. Evaporation of a non-ideal solution and its application to writing ink aging. *Forensic Sci. Int.* **2015**, *247*, 69–78. [CrossRef]
23. Turkan, B.; Etemoglu, A.B.; Can, M. Analysis of evaporative drying of thin ink films using high-velocity hot-air impinging jets: A comprehensive review. *Surf. Rev. Lett.* **2020**, *27*, 1950210. [CrossRef]
24. Wu, J.M.; Xu, Z.L.; Chen, Y.C.; Xue, Z.C.; Liu, L.L. Fluid dynamic analysis and parameter optimization of the drying box of gravure printing machines. *J. Vib. Shock* **2012**, *31*, 53–57. [CrossRef]
25. Wu, J.M.; You, L.; Liu, L.L.; Ma, L.E.; Zhang, Y.L. Optimization of the energy saving drying system for high-speed gravure printing machines. *Print. Technol.* **2014**, *10*, 24–26.
26. Liu, L.L.; You, L.; Xun, Z.C.; Wu, J.M. Numerical calculation and analysis of hot air in the drying box of gravure machine. *Packag. Eng.* **2015**, *36*, 87–94. [CrossRef]
27. Mujumdar, A.S. Book review: Handbook of industrial drying, Third Edition. *Dry. Technol.* **2007**, *25*, 1133–1134. [CrossRef]
28. Alpbaz, M.; Bilgesu, A.; Tutkun, O. The origin of the equation for the interfacial coefficient of heat transfer. *Fac. Sci. Univ. Ank. Serie B* **1988**, *34*, 114–128. [CrossRef]
29. Kaptay, G. The Gibbs equation versus the Kelvin and the Gibbs-Thomson equations to describe nucleation and equilibrium of nano-materials. *J. Nanosci. Nanotechnol.* **2012**, *12*, 2625–2633. [CrossRef] [PubMed]
30. Chemical Engineering Association. *Chemical Engineering Enchiridion*, 5th ed.; Marusha Corporation: Wakayama, Japan, 1988.
31. Sherwood, T.K. The curious history of the wet bulb hygrometer. *Chem. Can.* 1950.